https://doi.org/10.5281/zenodo.14844441

Thermal wellbore model—A geothermal drilling research tool

Thomas Gruner
SLB Cambridge Research, High Cross, Cambridge CB3 0EL, United Kingdom

Keywords: thermal modeling, geothermal drilling, heat management, well temperature control

Abstract

We have developed a versatile model that simulates the transient thermal behaviors of downhole tools and the surrounding environments when drilling into hot geothermal reservoirs. Special emphasis was placed on flexibility and full transparency during development. Assessing the correct functioning of the model at the most basic level—each individual equation—is essential to understanding and simulating the physics behind novel events or situations that are increasingly occurring in the geothermal domain.
The thermal wellbore model predicts the temperature evolution over time along and across certain solid parts of the bottomhole assembly (BHA), drillstring, and surrounding rock, as well as in the drilling fluid column (also known as mud) within both the drillpipe and annulus, respectively, when different parameters are altered. Those parameters include surface temperature, mud pit volume, mud flow rate, well diameter, depth, inclination, and geothermal temperature gradient; and physical properties of drillpipe, BHA, rock formation, and mud.
The model results will be validated against several different datasets. Beyond quasi-static solutions, particular emphasis is given to the simulation of highly dynamic drilling operations. Temperature profiles driven by mud losses and high-temperature influxes will also be presented. The model will reveal overlooked or neglected challenges and will point towards possible strategies on how to overcome or even use them. It is a new building block with which geothermal drilling will potentially become more reliable, more productive, and more cost-effective.

1. Introduction

A model simulating the thermal behavior of downhole environments and tools when drilling into hot geothermal reservoirs has been developed. The code our model is based on is designed for modeling multidomain physical systems, including the domains of thermal solid-state, thermal liquid, mechanical rotation, mechanical translation, and electrical. A broad range of scenarios can be modeled by tailored components using the modular principle. Comparable models do exist [1-5], but they are all too specialized and, hence, too inflexible to serve as a suitable research tool.

As a research tool, special emphasis was placed on flexibility and full transparency during development. This allows users to understand its operations and build confidence in its recommendations. Verifying the correct functioning of the model at the most basic level—each individual equation—is always possible. The presented model predicts the temperature evolution in certain solid parts of the bottomhole assembly (BHA) and drillstring, as well as in the mud column and the surrounding rock, when different parameters are altered. Those parameters include surface temperature, mud pit volume, mud flow rate, well section diameters, drillpipe thickness and material, BHA dimensions and material, true vertical well depth, measured depth, inclination, geothermal temperature gradient, formation material, mud properties, mud losses, and mud influx. The model is discretized along two spatial dimensions—axially, along the well trajectory, and

radially (from the center outwards: mud inside drillpipe, drillpipe, mud inside annulus, optional casing/cement, and formation rock shells). The thickness of the rock shell blocks grows exponentially away from the well. Our model's flexibility is essential to model events or situations that are increasingly occurring in the geothermal domain. The results capture the mechanical, hydraulic, and thermodynamic impacts of highly transient events and operations. In addition to conventional geothermal drilling, our model addresses the challenges associated with higher temperatures and larger depths (that is, higher enthalpies) as well as with the increasingly complex well geometries that our industry has been embarking on in recent years.

Drilling into rock reservoirs with higher formation temperatures and hydrostatic pressures generally has a positive impact on the amount of energy that can eventually be produced by the constructed geothermal system. Therefore, researching the interplay of the thermal properties of the drilling fluid, downhole tools, and surrounding formation is important for effectively managing the harsh environmental conditions that impact the complex electronics in a BHA. Identifying strategies to unlock the full potential of existing SLB technology while developing new tools in parallel, prioritizing limited resources, and optimizing thresholds to prevent dangerous and cost-intensive incidents are other performance indicators of our model.

2. Model formulation

The modeled wellbore system is radially divided into (i) mud inside the drillpipe, (ii) drillpipe, (iii) mud inside the annulus, (iv) optional casing/cement, and (v) formation rock shells (from the center outwards).

2.1 Solid elements—thermal solid-state

All solid-state elements are represented by thermal masses that are connected by conductive heat transfer elements. Here, the governing equations are:

$$Q = c \cdot m \frac{dT}{dt} \tag{1}$$

where Q is the heat flow; c is the specific heat of the material; m is the mass; T is the temperature; t is time, and

$$Q = \kappa \cdot \frac{A}{d}(T_A - T_B) \tag{2}$$

where κ is the thermal conductivity of the material; A is the area normal to the heat flow direction; d is the distance between layers, that is, the thickness of material; T_A is the temperature of layer A; T_B is the temperature of layer B.

2.2 Liquid elements—thermal liquid

Most fluid-bearing elements are represented by customized pipe elements. These blocks model pipe flow dynamics in a thermal liquid network due to viscous friction losses and convective heat transfer between the liquid and the pipe walls. The effects of dynamic compressibility and elevation are included. The pressure differential over the pipe will be caused by the pressure at the pipe ports, friction at the pipe walls, and hydrostatic changes due to any change in elevation. The pipe element contains a constant volume of liquid, which has a uniform internal temperature, T_i.

Temperature evolves based on the thermal capacity of this liquid volume. An imbalance of mass inflow and mass outflow in pipe elements can cause liquid to accumulate or diminish in the pipe. As a result, pressure in the pipe volume can rise and fall dynamically, providing some compliance to the system and modulating rapid pressure changes.

The pipe elements have ports A and B, which are the thermal liquid conserving ports associated with the pipe inlet and outlet. Three more ports (theses are H, H_i, and H_o) are the thermal conserving ports associated with the wall (simple pipes) as well as the inner and outer pipe walls (annual ducts), respectively.

The analytical Haaland correlation is an analytical approximation used to directly solve the Darcy–Weisbach friction equation [6]. This correlation is used here to model losses due to viscous wall friction Δp_v by aggregate equivalent length, which accounts for resistances due to nonuniformities as an added straight-pipe length that results in equivalent losses. The Haaland correlation is primarily used for Newtonian fluids, which have a constant viscosity that does not change with the rate of shear stress. Since water is currently used to model the drilling fluid, the Haaland correlation is sufficient.

The pressure differential over the pipe is due to the pressure at the pipe ports, hydrostatic changes due to any change in elevation, and viscous friction at the pipe walls:

$$p_A - p_B = \rho_i \, g \, \Delta z + \Delta p_v \tag{3}$$

where p_A is the pressure at a port A, p_B is the pressure at a port B, g is the value of the gravitational acceleration parameter, Δz the elevation differential between port A and port B, ($z_A - z_B$). ρ_i is the internal fluid density, which is measured at each pipe segment and comes from the database program NIST *Reference Fluid Thermodynamic and Transport Properties* (REFPROP version 10) [7]. At present, the drilling fluid is being simulated using the properties of pure water, meaning that additional mud weight is not implemented in the model. This is an option for later development. Δp_v is the pressure differential due to viscous friction ($\Delta p_{v,A} + \Delta p_{v,B}$), where $\Delta p_{v,A}$ and $\Delta p_{v,B}$ are the viscous friction pressure losses between the pipe volume center and ports A and B. For the half pipe adjacent to port A it is

$$\Delta p_{v,A} = \begin{cases} \lambda \nu \left(\dfrac{L + L_{eq}}{2}\right) \dfrac{\dot{m}_A}{2D^2 S}, & if\ Re_A < Re_{lam} \\ f_A \left(\dfrac{L + L_{eq}}{2}\right) \dfrac{\dot{m}_A |\dot{m}_A|}{2\rho D S^2}, & if\ Re_A \geq Re_{tur} \end{cases} \tag{4}$$

In the above equations, λ is the pipe shape factor, ν is the kinematic viscosity of the thermal liquid in the pipe, L_{eq} is the aggregate equivalent length of the local pipe resistances, D is the hydraulic diameter of the pipe, S is the pipe cross-sectional area, f_A is the Darcy friction factor in the pipe half adjacent to port A. Re_A is the Reynolds number at ports A. Re_{lam} is the Reynolds number above which the flow transitions to turbulent, and Re_{tur} is the Reynolds number below which the flow transitions to laminar. The equation for $\Delta p_{v,B}$ has the same structure.

Heat transfer between the fluid and pipe wall occurs through convection Q_{Conv} and conduction Q_{Cond}, where the net heat flow rate is $Q_H = Q_{Conv} + Q_{Cond}$.

Heat transfer due to conduction is:

$$Q_{Cond} = \frac{\kappa_I \cdot S_H}{D} (T_H - T_i) \tag{5}$$

where D is the nominal hydraulic diameter ($D_0 - D_i$); κ_I is the thermal conductivity of the thermal liquid, defined internally for each pipe segment; S_H is the surface area of the pipe wall; T_H is the pipe wall temperature; T_i is the fluid temperature at the internal node of the block.

Heat transfer due to convection is:

$$Q_{Conv} = c_{p,avg} \cdot \dot{m}_{avg} \cdot (T_H - T_{in}) \left[1 - \exp\left(-\frac{h_{coeff} \cdot S_H}{c_{p,avg}\dot{m}_{avg}}\right)\right] \tag{6}$$

where $c_{p,avg}$ is the average fluid-specific heat, which the block calculates using REFPROP [7]; $\dot{m}_{avg}$ is the average mass flow rate through the pipe; T_{in} is the fluid inlet port temperature; h_{coeff} is the pipe heat transfer coefficient ($h_{coeff} = (Nu \cdot \kappa_{avg})/D$ with κ_{avg} is the average thermal conductivity of the thermal liquid over the entire pipe and Nu is the average Nusselt number in the pipe).

In the case of circular pipe elements, the following so-called Gnielinski correlation is used to calculate the average Nusselt number [8]:

$$Nu = \frac{(f/8)(Re - 1000)Pr}{1 + 12.7\sqrt{f/8}\,(Pr^{2/3} - 1)} \tag{7}$$

where *f* is the average Darcy friction factor, $f = (0.79\ln(Re) - 1.64)^{-2}$, Re is the Reynolds number, and Pr is the Prandtl number.

In the case of annular ducts, the average Nusselt number is calculated as:

$$Nu = \frac{(f/8)(Re - 1000)Pr}{1 + 12.7\sqrt{f/8}(Pr^{2/3} - 1)} \left[1 + \left(\frac{D}{L}\right)^{2/3}\right] f_{ann} \cdot K \tag{8}$$

where D is the hydraulic diameter; L is the length of the pipe segment, f_{ann} is the friction factor of the annular duct. f_{ann} depends on the annular diameter ratio $a = D_i / D_o$:

$$f_{ann} = (1.8 \log Re^* - 1.5)^{-2} \tag{9}$$

where

$$Re^* = Re \frac{(1 + a^2)\ln(a) + (1 - a^2)}{(1 - a^2)\ln(a)} \tag{10}$$

Since the simulated drilling fluid varies it properties with temperature, different Prandtl numbers are considered:

$$K = \left(\frac{Pr_b}{Pr_w}\right)^{0.11} \tag{11}$$

where Pr_b is the Prandtl number of the mud at bulk temperature T_i and Pr_w at wall temperature, respectively.

The remaining elements in the thermal liquid domain are flow rate sources, check valve, and sudden area changes. In 2014, Volker Gnielinski developed correlations for calculating heat transfer coefficients for turbulent flow in annuli [9]. These correlations are the basis for modeling the annular duct properties within the model.

3. Benchmarking and validation

Extrinsic evaluation involves assessing the model's performance in real-world applications. It provides a practical measure of its effectiveness. By comparing our model in different scenarios, we obtain a sound overview of the model's strengths and areas for improvement.

3.1 Test case A—Shallow well

Test case A is based on data from the Utah Forge project [10]. The well is approximated as truly vertical with a wellbore diameter of 22.225 cm. It is drilled with conventional drillpipes (CDP) ($\varnothing_{OD}$ = 12.7 cm, d_{wall} = 0.91 cm, ρ_{CDP} = 7850 kg m^{-3}, $c_{p,\,CDP}$ = 490 Jkg^{-1}K^{-1}, κ_{CDP} = 45 Wm^{-1}K^{-1}) into granite (ρ_{rock} = 2800 kg m^{-3}, $c_{p,\,rock}$ = 930 Jkg^{-1}K^{-1}, κ_{rock} = 2.31 Wm^{-1}K^{-1}). A surface temperature of 40°C together with a geothermal gradient of 69.1°C km^{-1} result in far-field rock temperature of around 220°C at the bottom hole. Pure water with a surface flow rate of 37.86 ls^{-1} is used to approximate the drilling fluid.

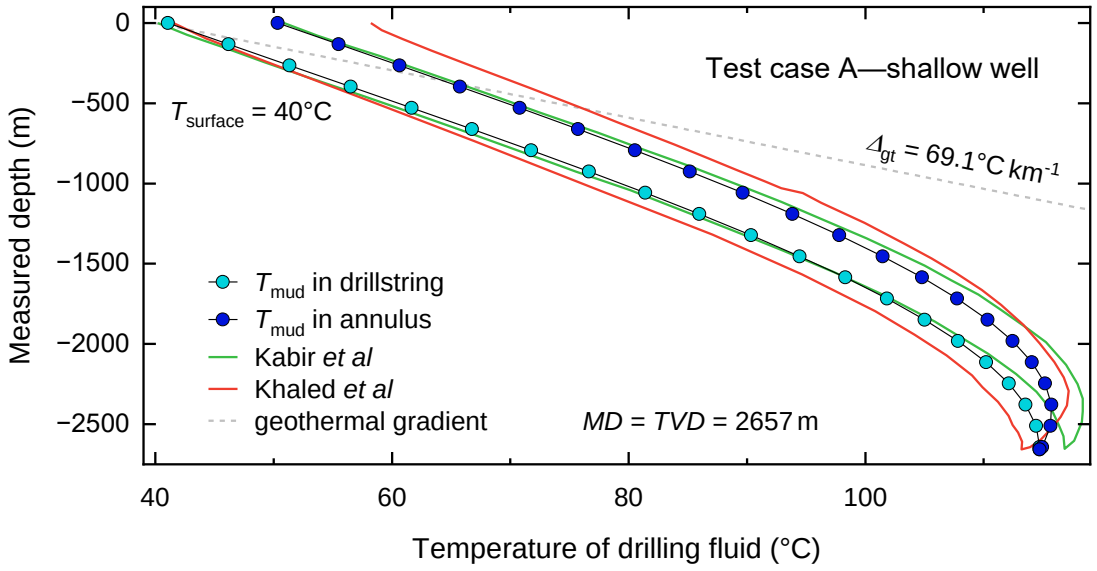

Fig. 1: Temperature profile of (quasi) steady-state simulation. For test case A—a shallow vertical well with a measured depth of 2657 m—the bottomhole circulation temperature reaches about 115°C. These results are validated by the good match with reported data [2, 3].

For test case A, the more resource-friendly (quasi) steady-state approach to simulation was chosen. The entire well already exists at the beginning of the simulation; there is no direct modeling of the rate of penetration (ROP). Below, a dynamic method will be described that captures highly transient events. The results in Fig. 1 show the temperature profiles that occur after 24 hours of circulation. Interestingly, the maximal temperature in the entire mud system is observed about 230 m above the bottomhole in the annulus. Comparing these results with other models [3] and an experimentally validated analytical solver [2] shows very close agreements. Temperature differences between the simulations of only +1.7°C [3] and -2°C [2], respectively, at bottomhole validate our model in case A.

3.2 Test case B—deep well

Test case B mimics a deep well with a measured depth of 8600 m drilled in West Texas, USA [11]. It was chosen to have a very similar bottomhole far-field rock temperature (220°C) although the

geothermal gradient of 24°C km^{-1} is much smaller than in case A. In this model, the surface air temperature (T_{air} = 40°C) and the surface rock temperature ($T_{surface\ rock}$ = 17°C) are different, resulting in a slightly distorted temperature profile (see Fig. 2). The rest of the input parameters are equal to test case A (these are $Ø_{wellbore}$ = 22.225 cm, $Ø_{OD\ drillpipe}$ = 12.7 cm, $d_{drillpipe\ wall}$ = 0.91 cm, ρ_{CDP} = 7850 kg m^{-3}, $c_{p,\ CDP}$ = 490 Jkg^{-1}K^{-1}, κ_{CDP} = 45 Wm^{-1}K^{-1}, ρ_{rock} = 2800 kg m^{-3}, $c_{p,\ rock}$ = 930 Jkg^{-1}K^{-1}, κ_{rock} = 2.31 Wm^{-1}K^{-1}.

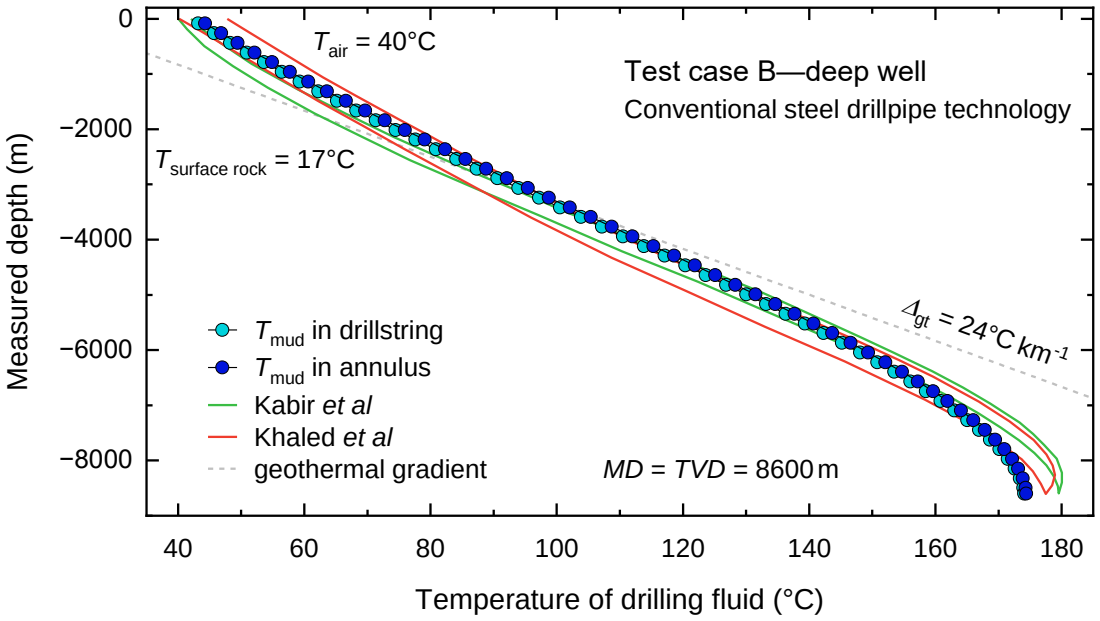

Fig. 2: Temperature profile of (quasi) steady-state simulation. For the test case B, the bottomhole circulation temperature reaches about 175°C. This is close to the threshold of what is possible to drill with standard 175°C-rated tools. The results are validated against third-party models reported elsewhere [2, 3].

The results of simulation B are shown in Fig. 2. As in case A, the deviation between our model and the models reported earlier is only a few degrees Celsius (-3.1°C [3] and -5.1°C [2], respectively). The bottomhole circulation temperature, and thus almost inevitably the tool temperature, rises very close to the limit of 175°C. 175°C is an important threshold temperature for many drilling tools. Once the delicate downhole tools are exposed to higher temperatures than they are rated for, they will fail or be damaged with high probability. One measure to overcome this is using insulated drillpipe technology.

4. Insulated drillpipe technology

After validating our model (see Fig. 1 and Fig. 2), the limitations of conventional drillpipe (CDP) are studied. Assuming that it is possible to change the drillstring from conventional technology (with $d_{CDP\ wall}$ = 0.91 cm and κ_{CDP} = 45 Wm^{-1}K^{-1}) to insulated drillpipe (IDP), with $d_{IDP\ wall}$ = 2.45 cm and κ_{CDP} = 3.12 Wm^{-1}K^{-1}) while keeping all other parameters equal to those already discussed for case B, our model can be used to show the differences between the technologies. Fig. 3 shows the impact on the bottomhole circulation temperature. The value of around 175°C, when using CDP, could be reduced by 63°C to meet 112°C in the IDP case. Here, it is possible to even use 125°C-rated electronics in the BHA to drill the project. This also generally increases the longevity of any tool because the harmful thermal input can be kept permanently low.

Furthermore, the results show that the additional energy extracted from the rock formation causes the drilling fluid in the surface mud pit to heat up noticeably. The surface facilities must be prepared for this, for instance by active mud chilling. Otherwise, hot mud will be sent down, which will no longer be able to develop a sufficient cooling effect downhole.

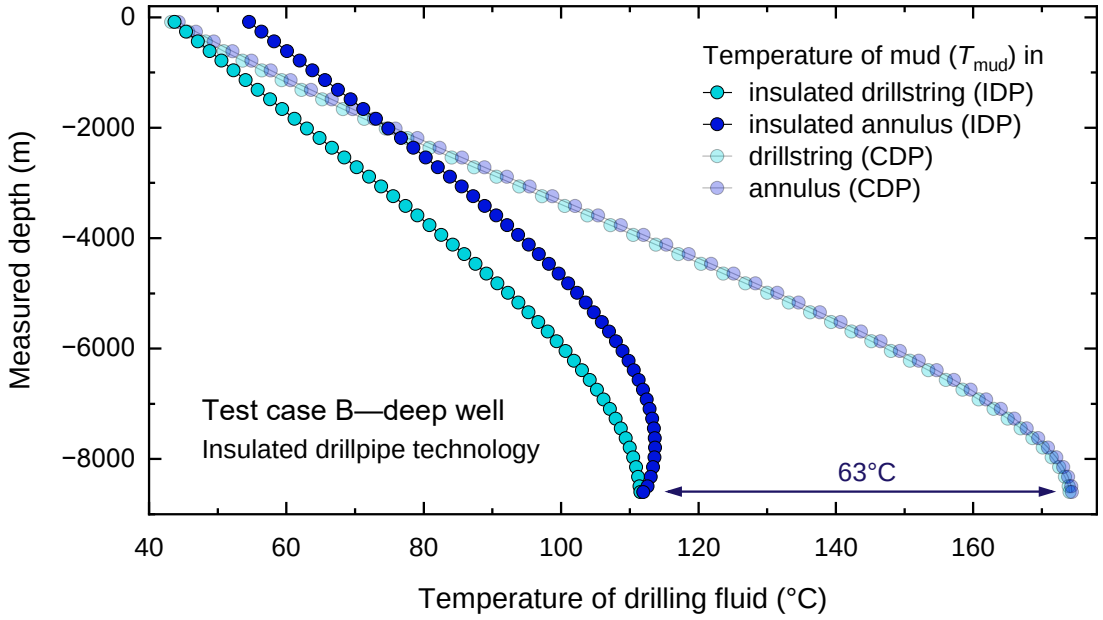

Fig. 3: Temperature profile when changing from CDP ($d_{CDP\ wall}$ = 0.91 cm, κ_{CDP} = 45 $Wm^{-1}K^{-1}$) to IDP ($d_{IDP\ wall}$ = 2.45 cm, κ_{CDP} = 3.12 $Wm^{-1}K^{-1}$) technology. A reduction of about 63°C is shown, making it possible to use 125°C-rated electronics in that hypothetical project.

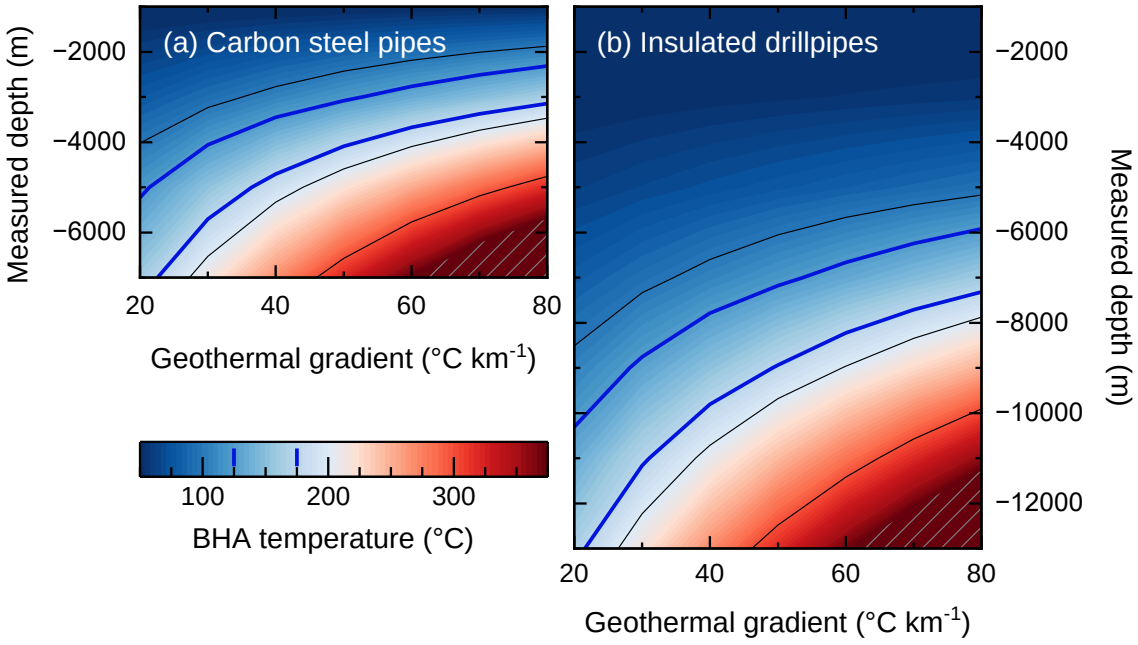

Fig. 4: Comparison of conventional drillpipe (CDP, κ_{CDP} = 45 $Wm^{-1}K^{-1}$) with insulated drillpipe (IDP, κ_{CDP} = 3.12 $Wm^{-1}K^{-1}$) technology. The color code represents the simulated temperature within the BHA. On the vertical axis, the measured depth is shown, while on the horizontal axis, the geothermal gradient is shown. Both quantities determine the temperature of the surrounding rock formation. The deeper and the higher the geothermal gradient, the hotter the rock reservoir. The two blue lines represent two threshold temperatures of standard downhole electronics, that is, 125°C and 175°C, respectively. (a) With traditional carbon steel drillpipe technology, it is not safely possible to drill to depths below the blue lines. (b) With insulated pipe technology, the thresholds are pushed towards greater depths and higher geothermal gradients. In this example, it is possible to drill to at least 6000 m without damaging 125°C-rated electronics.

The results of nearly one hundred separate simulations, similar to those discussed in Fig. 2 and Fig. 3, are combined to create the color plot displayed in Fig. 4. The plots show the maximum drillable depths for a given geothermal gradient, where the BHA temperature stays below 125°C and 175°C, respectively. These widespread thresholds are marked by two solid blue lines. The simulations clearly show that it is possible to drill to greater depths and geothermal gradients while maintaining the required temperature ranges when IDP technology is used instead of CDP.

5. Transient drilling operations

The capability of the model to simulate dynamic thermal responses that occur when drilling a hypothetical vertical well with a ROP of 12 mh^{-1} is discussed in this section. The measured depth of 5 km is reached after about 417 hours or about 17 days of uninterrupted drilling. The use of IDP technology is considered ($Ø_{wellbore}$ = 21.59 cm, $Ø_{OD\ drillpipe}$ = 12.7 cm, $d_{drillpipe\ wall}$ = 0.91 cm, $\kappa_{drillpipe}$ = 2.6 $Wm^{-1}K^{-1}$). Water with a flow rate equal to 41.7 ls^{-1} is used to approximate the drilling fluid. As in all previously discussed cases, the properties of granite are used for the surrounding rock. T_{air} is set to 30°C. At this temperature, the heat exchange in the mud pit happens. A soil temperature of $T_{surface\ rock}$ = 10°C together with the geothermal gradient Δ_{gt} = 50°C km^{-1} results in a far-field rock temperature of 260°C at a depth of 5000 m.

In the transient model, time-dependent precooling of the formation above the bottom of the hole is mimicked. The chronological order and the time span at which each rock segment is exposed to the mud's thermal drain are determined by the rate of penetration. The upper parts of the formation are in longer thermal contact with the drilling fluid than the lower section, which is drilled later. Sequential snapshots of the mud temperatures inside the drillstring and inside the annulus are shown in Fig. 5. The results of the transient model at an elapsed time $t_{elapsed}$ = 416.6 hours are slightly distorted when comparing them with the quasi steady-state approach discussed above (not shown). However, the main point and the great advantage of using a transient model are the highly dynamic events and operations that happen on the time scale of a couple of seconds.

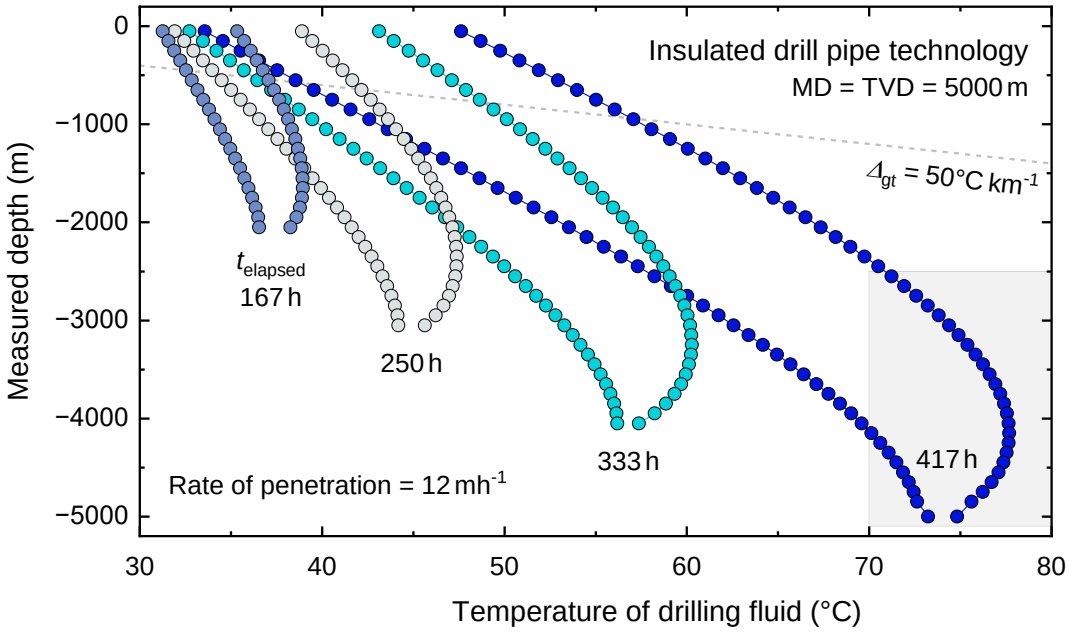

Fig. 5: Sequential snapshots of the mud temperatures inside the drillstring and inside the annulus are shown when drilling a well with $Ø_{wellbore}$ = 21.59 cm to a measured depth of 5000 m. The dark blue data marks the end of the drilling phase at an elapsed time of $t_{elapsed}$ = 416.6 hours. In this model, the shallower rock layers have approximately 400 hours longer thermal contact with the drilling fluid than the layers at the very bottom of the well.

One example of such an event is a sudden influx of hot formation fluid from the surrounding rock into the wellbore. The temperature of that fluid is typically very high. In this scenario, it is assumed to be 260°C, which reflects the far-field rock temperature at that depth. During an influx, there is a risk that the circulating mud is not efficient enough to thermalize the hot influx fluids to maintain the wellbore below temperature limits or to prevent the flashing of return fluids at the surface.

In the case discussed in Fig. 6, a volume of 1.8 m^3 of rock water flows into the wellbore at the very bottom. After a short run-up phase of 12 s, during which the flow rate increases constantly to 16.7 ls^{-1}, the influx lasts for 1.8 min. After a ramp-down phase of 12 s, the influx ceases. However, the impact on the temperature in the wellbore persists for a much longer time afterward.

Our model captures the key features associated with rapid influxes. During the influx, the mud temperature around the BHA increases quickly to a maximum value of 116°C. The value does not reach 260°C since the mud coming in from above dilutes the influx and thus cools it down. The heat wave then moves upwards in the annulus. Even a moderate event, lasting only around two minutes, causes a short-term temperature rise in the annular fluid of around 40°C. Our model can be seamlessly extended, enabling a prediction of the heat impact through the architecture of the BHA to the electronics.

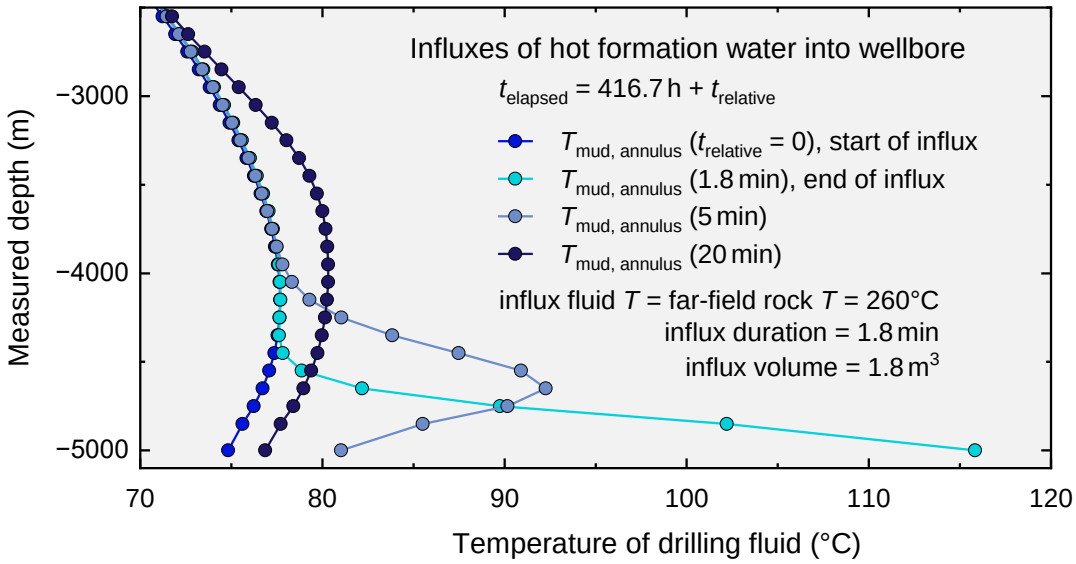

Fig. 6: Modeled results of formation influx on the annular temperature profile. The undisturbed temperature profile at the start of the influx is identical to the correspondent data at an elapsed time of $t_{elapsed}$ = 416.6 hours in Fig. 5.

6. Model verification—Intrinsic evaluation

The verification of the model is an essential part of ensuring its reliability and robustness. The model is evaluated with a set of different initial conditions, including the variation of the number of drillpipe segments along the trajectory of the wellbore (n_{mesh}).

The model input parameters are as follows: n_{mesh} = 4 to 100; $Ø_{wellbore}$ = 22.225 cm, MD = 5000 m (vertical well), ROP = 10 mh^{-1}, mud flow rate is 10 ls^{-1} (properties of pure water are used), T_{air} = $T_{surface\ rock}$ = 18°C, geothermal gradient Δ_{gt} = 50°C km^{-1}. Granite is the surrounding rock. IDP technology is simulated ($Ø_{OD\ drillpipe}$ = 12.7 cm, $d_{drillpipe\ wall}$ = 2.454 cm, $\kappa_{drillpipe}$ = 3.12 $Wm^{-1}K^{-1}$).

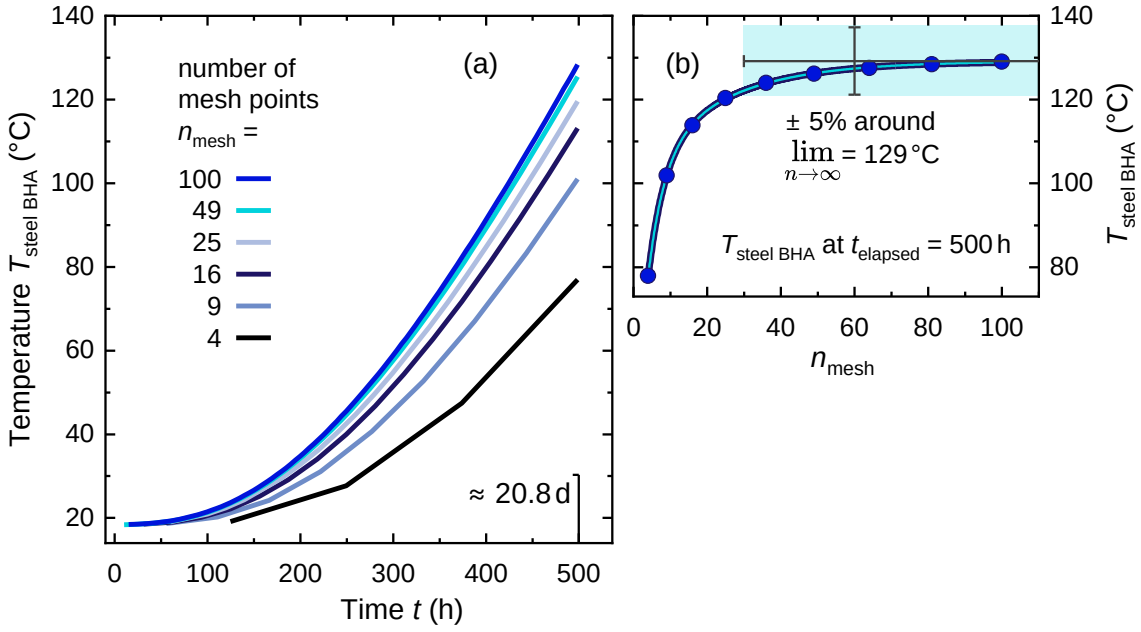

Fig. 7: Model verification. (a) At each time step in the simulation, the number of segments along the wellbore trajectory (proportional to n_{mesh}) has an impact on $T_{steel\ BHA}$. After an elapsed time, t = 500 hours, simulations with different mesh sizes result in different $T_{steel\ BHA}$ values. (b) The higher the number of segments (n_{mesh}) the smaller the relative differences between the simulated temperatures. For n_{mesh} > 30, the simulated $T_{steel\ BHA}$ is within a range of ±5% around the extrapolated value of 129°C.

The temperature of the inner BHA steel layer, $T_{steel\ BHA}$, was selected for comparison. Simulated results of $T_{steel\ BHA}$ versus elapsed time, t, are shown in Fig. 7a. After an elapsed time, t = 500 hours, simulations with different mesh sizes result in artificially different $T_{steel\ BHA}$(500 hours) values. An overview of these values is plotted against the mesh number in Fig. 7b. These data are fitted with a combination of two exponential decay functions added together:

$$T_{\text{steel BHA}}(n_{\text{mesh}}) = T_0 + T_1\left[1 - \exp\left(-\frac{n_{\text{mesh}}}{b_1}\right)\right] + T_2\left[1 - \exp\left(-\frac{n_{\text{mesh}}}{b_2}\right)\right] \quad (12)$$

The solid line in Fig. 7b shows this fit. The sum of the initial value (T_0) and the amplitudes of the two exponential decay functions (T_1 and T_2) determines the saturation value, which is about 129°C for the considered scenario. A corridor of ±5% around the absolute extrapolated temperature is drawn. For n_{mesh} > 30, every simulated $T_{steel\ BHA}$(500 hours) value is within a range of ±5% around the extrapolated value, indicating that simulations with n_{mesh} ≈ 30 are sufficient to model standard drilling, workover, and well-control operation with a high accuracy. n_{mesh} ≈ 30 sets the minimum model mesh size for nearly all simulations described above.

7. Conclusion

The presented thermal wellbore model predicted temperature profiles, heat flows, and fluid flows while drilling geothermal wells. The model was exposed to different environments and data distributions to ensure that its performance is not overly dependent on specific conditions.

A model that maintains consistent performance across diverse environments can be deemed more adaptable. Considering its adaptability and flexibility, our model is an ideal research tool. It was developed to handle even unforeseen special circumstances that will increasingly occur in the

geothermal domain. Accurately simulating thermal hydraulic wellbore properties across different time and length scales makes this model a further building block that will help ensure SLB's technology remains future-proof for the coming decades.

The presented version of the model could be seamlessly upgraded to simulate more complex structures. This will result in innovative heat management strategies, which guarantee a safe, sustainable, and cost-effective use of a wider selection of downhole tools that work reliably even under extreme thermal conditions.

Acknowledgements

The author is indebted to N. Heaton, H. M. Panayirci, E. Muyzert, and T. Grimble for fruitful discussions.

References

[1] Goura, N., Champness, S., & Fitzpatrick, C.: Managing Temperature to Enable Directional Drilling to 500°C Without Losses, Geothermal Resources Council Transactions, vol. 47, 2023.

[2] Kabir, C. S., Hasan, A. R., Kouba, G. E., & Ameen, M. M.: Determining Circulating Fluid Temperature in Drilling, Workover, and Well Control Operations, presented at the 1992 SPE Annual Technical Conference & Exhibition, Washington, DC, USA, 1996.

[3] Khaled, M. S., Wang, N., Ashok, P., & van Oort, E.: Downhole heat management for drilling shallow and ultra-deep high enthalpy geothermal wells, Geothermics, vol. 107, 2023, doi: 10.1016/j.geothermics.2022.102604.

[4] Fallah, A., et al.: Temperature dynamics and its effects on gas influx handling during managed pressure drilling operations, Journal of Natural Gas Science and Engineering, vol. 83, 2020, doi: 10.1016/j.jngse.2020.103614.

[5] Abdelhafiz, M. M., Oppelt, J., & Hegele, L. A.: Thermal Analysis of the Wellbore System During Drilling Operations Using an Improved Drilling Simulator, presented at Day 3 Wed, 2nd Nov, 2022.

[6] Haaland, S. E.: Simple and Explicit Formulas for the Friction Factor in Turbulent Pipe Flow, Journal of Fluids Engineering, vol. 105, no. 1, pp. 89-90, 1983, doi: 10.1115/1.3240948.

[7] Lemmon, E. W., Huber, M. L., McLinden, M. O., & Bell, I.: NIST Reference Fluid Thermodynamic and Transport Properties Database (REFPROP): Version 10.

[8] Gnielinski, V.: Neue Gleichungen für den Wärme- und den Stoffübergang in turbulent durchströmten Rohren und Kanälen, Forschung im Ingenieurwesen A, vol. 41, no. 1, pp. 8-16, 1975/01/01 1975, doi: 10.1007/BF02559682.

[9] Gnielinski, V.: Turbulent Heat Transfer in Annular Spaces - A New Comprehensive Correlation, Heat Transfer Engineering, vol. 36, no. 9, pp. 787-789, 2015/06/13 2014, doi: 10.1080/01457632.

[10] Simmons, S., et al.: Update on the Geoscientific Understanding of the Utah FORGE Site, in 44th Workshop on Geothermal Reservoir Engineering, Stanford, California, 2019, vol. SGP-TR-214.

[11] Erdlac, Richard J.: A Resource Assessment Of Geothermal Energy Resources For Converting Deep Gas Wells In Carbonate Strata Into Geothermal Extraction Wells: A Permian Basin Evaluation, United States,2006. [Online]. Available: https://doi.org/10.2172/893183.

Address, SLB Cambridge Research, High Cross, Cambridge CB3 0EL, United Kingdom
E-Mail, TGruner@slb.com